Inorganic Chemistry

Article

pubs.acs.org/IC

Intensely Luminescent Homoleptic Alkynyl Decanuclear Gold(I) Clusters and Their Cationic Octanuclear Phosphine Derivatives

Igor O. Koshevoy,*[,†] Yuh-Chia Chang,[‡] Antti J. Karttunen,[†] Stanislav I. Selivanov,[§] Janne Jänis,[†] Matti Haukka,[†] Tapani Pakkanen,[†] Sergey P. Tunik,[§] and Pi-Tai Chou*[,‡]

[†]Department of Chemistry, University of Eastern Finland, Joensuu, 80101, Finland

[‡]Department of Chemistry, National Taiwan University, Taipei 106, Taiwan

[§]Department of Chemistry, St. Petersburg State University, Universitetskii pr. 26, 198504, St. Petersburg, Russia

Supporting Information

ABSTRACT: Treatment of $Au(SC_4H_8)Cl$ with a stoichiometric amount of hydroxyaliphatic alkyne in the presence of NEt_3 results in high-yield self-assembly of homoleptic clusters $(AuC_2R)_{10}$ (R = 9-fluorenol (**1**), diphenylmethanol (**2**), 2,6-dimethyl-4-heptanol (**3**), 3-methyl-2-butanol (**4**), 4-methyl-2-pentanol (**4**), 1-cyclohexanol (**6**), 2-borneol (**7**)). The molecular compounds contain an unprecedented catenane metal core with two interlocked 5-membered rings. Reactions of the decanuclear clusters **1**−**7** with gold−diphosphine complex $[Au_2(1,4\text{-}PPh_2{-}C_6H_4{-}PPh_2)_2]^{2+}$ lead to octanuclear cationic derivatives $[Au_8(C_2R)_6(PPh_2{-}C_6H_4{-}PPh_2)_2]^{2+}$ (**8**−**14**), which consist of planar tetranuclear units $\{Au_4(C_2R)_4\}$ coupled with two fragments $[AuPPh_2{-}C_6H_4{-}PPh_2(AuC_2R)]^+$. The titled complexes were characterized by NMR and ESI-MS spectroscopy, and the structures of **1**, **13**, and **14** were determined by single-crystal X-ray diffraction analysis. The luminescence behavior of both Au^I_{10} and Au^I_8 families has been studied, revealing efficient room-temperature phosphorescence in solution and in the solid state, with the maximum quantum yield approaching 100% (**2** in solution). DFT computational studies showed that in both Au^I_{10} and Au^I_8 clusters metal-centered Au → Au charge transfer transitions mixed with some π-alkynyl MLCT character play a dominant role in the observed phosphorescence.

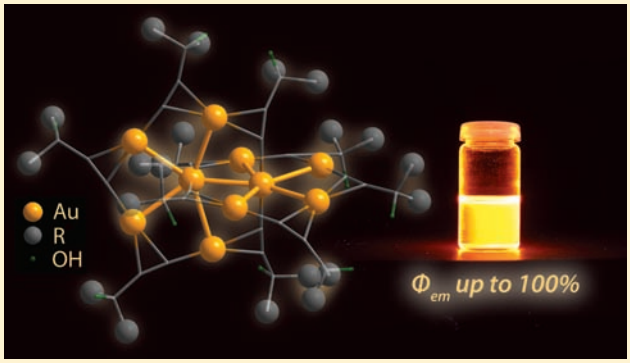

INTRODUCTION

Alkynyl gold complexes attract considerable attention due to their rich photoluminescent properties,[1] which, in particular, serve as a basis for their potential applications in luminescent chemosensing[2] and fabrication of optoelectronic devices.[3] Due to the pronounced tendency of the gold ions to form metal−metal (aurophilic) bonds,[4] these compounds often aggregate in the solid state and in solution to give intriguing polynuclear assemblies of various structural types.[4b,5] Homoleptic alkynyl gold complexes (AuC_2R), where the σ,π-bridging organic ligand saturates at least two coordination vacancies of the Au^I ion, usually form poorly soluble polymeric materials, which are difficult to characterize in detail.[5c,6] Despite the lack of structural knowledge of this class of compounds, preparation of $(AuC_2R)_n$ polymers has been well established to provide important precursors, which are widely employed in the synthesis of numerous heteroleptic organometallic derivatives of general formula $LAuC_2R$ (L = phosphine, pyridine, isonitrile).[6b,7]

Structural and spectroscopic information on the homoleptic alkynyl species $(AuC_2R)_n$ is very scarce. To the best of our knowledge, satisfactory characterization has been so far reported for three compounds only. $(AuC_2{-}Bu^t)_{12}$ was shown to form a catenane system consisting of two interlocked six-membered rings (Figure 1), which is retained in solution.[5a] Furthermore, employment of alkynylcalix[4]crown-6 ligand led to a planar tetranuclear gold cluster exhibiting intense luminescence.[5b] Finally, the polymeric structure of the phenylacetylenic complex $(AuC_2Ph)_n$ was proven by X-ray powder diffraction analysis, revealing a layered Au···Au honeycomb network with $-C_2Ph$ pillars.[5c] These few diverse examples clearly suggest that the nature of the organic group of the alkyne ligand, i.e., stereochemical bulkiness and electronic properties, could play a significant role in the assembly of (AuC_2R) units via aurophilic interactions and Au−π-C≡CR bonding, leading to various geometrical arrangements of the resulting molecules or solid phases.

In our recent study of a family of Au−Cu clusters bearing aliphatic alkyne ligands,[8] we noticed that some of the starting $(AuC_2OHR)_n$ compounds with hydroxyaliphatic organic groups exhibited decent solubility in common organic solvents, providing solutions of intense yellow color. These observations suggested the possible formation of molecular polymetallic aggregates and inspired us to carry out a more detailed study of

Received: April 26, 2012
Published: June 11, 2012

   dx.doi.org/10.1021/ic300856h | Inorg. Chem. 2012, 51, 7392−7403

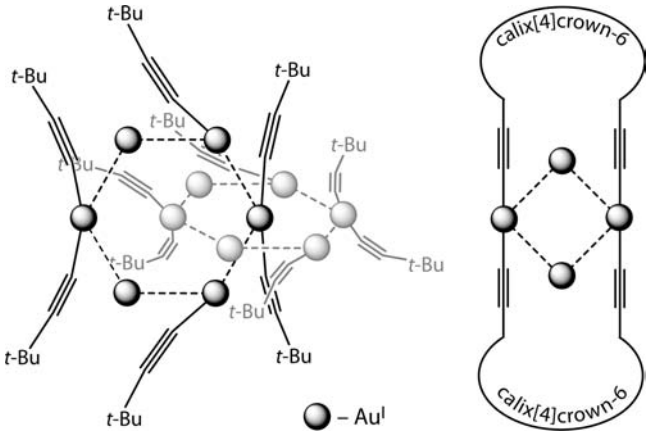

Figure 1. Representation of the previously reported homoleptic alkynyl molecular clusters of Au^{I}: [2]catenane−$[(AuC_2-Bu^t)_6]_2$ and $[Au_2(C_2)_2$−alkynylcalix[4]crown-6$]_2$.[5a,b]

the series of $(AuC_2OHR)_n$ complexes. Here we investigate the effect of the constituting organic ligands on the properties of the $(AuC_2OHR)_n$ complexes and the possibility of transforming the homoleptic species into the cationic phosphine derivatives using the method we communicated earlier.[5f]

EXPERIMENTAL SECTION

General Comments. Au(tht)Cl (tht = tetrahydrothiophene),[9] 1,4-bis(diphenylphosphino)benzene,[10] and 2-*endo*-ethynylborneol[11] were obtained according to the literature methods. $[Au_2(1,4\text{-}PPh_2C_6H_4PPh_2)_2]^{2+}$ as PF_6^- and ClO_4^- salts were obtained by treatment of a stoichiometric mixture of $Au(tht)Cl/PPh_2C_6H_4PPh_2$ with $AgPF_6$ or $AgClO_4$, respectively, analogously to the published procedures.[12] Other reagents and solvents were used as received. The solution 1D ^1H, ^{31}P NMR, and $^1H-^1H$ COSY (and J-COSY), $^1H-^1H$ NOESY, and $^1H-^{13}C$ HSQC spectra were recorded on Bruker Avance 400 and Bruker DPX 300 spectrometers. Mass spectra were measured on a Bruker APEX-Qe ESI FT-ICR instrument in the negative- and positive-ion modes. Microanalyses were carried out in the analytical laboratory of the University of Eastern Finland.

Synthesis of $(AuC_2R)_n$ Complexes 1−7. Au(tht)Cl (100 mg, 0.312 mmol) was dissolved in acetone (15 cm^3), and a solution of the corresponding HC_2R (ca. 0.4 mmol) in acetone (3 cm^3) was added in one portion followed by neat NEt_3 (5 drops, ca. 40 mg). The reaction mixture was stirred for 30 min in the absence of light and evaporated. Subsequent workup gave **1**−**7** as yellow solids (81−95%). The detailed description of the synthesis is given in the Supporting Information.

$(AuC_2C_{13}H_9O)_{10}$ (1). Bright yellow microsrystalline material (89%). ES MS (m/z): $[M - H^+]^-$ 4019.4 (calcd 4019.3). ^1H NMR (acetone-d_6, 298 K; δ): major isomer, OH signals 5.95 (s, 4H), 5.92 (s, 2H), 5.40 (s, 4H); three groups of alkynyl ligands, group 1 7.67 (d, 8H, J(H−H) 7.5 Hz), 7.17 (d, 8H, J(H−H) 7.5 Hz), 7.01 (dd, 8H, J(H−H) ca. 7.5 Hz), 6.86 (dd, 8H, J(H−H) 7.5 Hz); group 2 8.04 (d, 8H, J(H−H) 7.5 Hz), 7.83 (d, 8H, J(H−H) 7.5 Hz), 7.48 (dd, 8H, J(H−H) ca. 7.5 Hz), 7.31 (dd, 8H, J(H−H) 7.5 Hz); group 3 8.05 (d, 4H, J(H−H) 7.5 Hz), 7.93 (d, 4H, J(H−H) 7.5 Hz), 7.56 (dd, 4H, J(H−H) ca. 7.5 Hz), 7.42 (dd, 4H, J(H−H) 7.5 Hz); minor isomer, OH signals 5.94 (s); alkynyl ligands 7.88 (d, 8H, J(H−H) 7.5 Hz), 7.75 (d, 8H, J(H−H) 7.5 Hz), 7.37 (dd, 8H, J(H−H) 7.5 Hz), 7.36 (dd, 8H, J(H−H) 7.5 Hz). Anal. Calcd for $Au_{10}C_{150}H_{90}O_{10}$: C, 44.80; H, 2.26. Found: C, 44.89; H, 2.51.

$(AuC_2C_{13}H_{11}O)_{10}$ (2). Yellow-orange solid (92%). ES MS (m/z): $[M - H^+]^-$ 4039.5 (calcd 4039.5). ^1H NMR (acetone-d_6, 298 K; δ): OH signals 6.22 (s, 4H), 6.13 (s, 4H), 5.52 (s, 2H); three groups of alkynyl ligands, group 1 7.71 (m, *ortho*-H, 16H, J(H−H) ca. 7.2 Hz), 7.00 (dd, *meta*-H, 16H, J(H−H) ca. 7.2 Hz), 6.93 (tt, *para*-H, 8H, J(H−H) 7.2 and 2.1 Hz); group 2 7.54 (m, *ortho*-H, 16H, J(H−H) ca. 7.1 Hz), 7.01−7.14 (ABX system of *meta-para*-H, 24H); group 3 7.48 (m, *ortho*-H, 8H, J(H−H) ca. 7.2 Hz), 7.08−7.20 (ABX system of *meta-para*-H, 12H). Anal. Calcd for $Au_{10}C_{150}H_{110}O_{10}$: C, 44.57; H, 2.74. Found: C, 44.93; H, 2.97.

$(AuC_2C_9H_{19}O)_{10}$ (3). Bright yellow-orange solid (81%). ES MS (m/z): $[M - H^+]^-$ 3640.1 (calcd 3640.1). ^1H NMR (acetone-d_6, 298 K; δ): OH signals 4.34 (s, 4H), 4.02 (s, 2H), 3.65 (s, 4H); three groups of alkynyl ligands (COSY-DQF, HSQC, and J-COSY routines were also used for signal assignment) group 1 1.068 (d, CH_3, 24H, J(H−H) 6.7 Hz), 1.047 (d, CH_3, 24H, J(H−H) 6.7 Hz), 2.195 (m, CH, 8H, J(H−H) 6.7, 5.7, and 7.0 Hz), 1.83 (dd, CH_2, 8H, J(H−H) 14.0 and 5.7 Hz), 1.665 (dd, CH_2, 8H, J(H−H) 14.0 and 7.0 Hz); group 2 1.044 (d, CH_3, 24H, J(H−H) 6.7 Hz), 1.032 (d, CH_3, 24H, J(H−H) 6.7 Hz), 2.135 (m, CH, 8H, J(H−H) 6.7, 5.7, and 7.0 Hz), 1.836 (dd, CH_2, 8H, J(H−H) 14.0 and 5.7 Hz), 1.794 (dd, CH_2, 8H, J(H−H) 14.0 and 7.0 Hz); group 3 1.061 (d, CH_3, 12H, J(H−H) 6.7 Hz), 1.043 (d, CH_3, 12H, J(H−H) 6.7 Hz), 2.184 (m, CH, 4H, J(H−H) 6.7, 5.7, and 7.0 Hz), 1.877 (dd, CH_2, 4H, J(H−H) 14.0 and 5.7 Hz), 1.803 (dd, CH_2, 4H, J(H−H) 14.0 and 7.0 Hz).

$(AuC_2C_5H_{11}O)_{10}$ (4). Yellow solid (95%). ES MS (m/z): $[M - H^+]^-$ 3079.5 (calcd 3079.5). ^1H NMR (acetone-d_6, 298 K; δ): OH signals 4.86 (s, 4H), 4.55 (s, 4H), 4.54 (s, 2H); three groups of alkynyl ligands (COSY-DQF, HSQC, and J-COSY routines were also used for signals assignment) group 1 1.088 (d, CH_3, 12H, J(H−H) 6.7 Hz), 1.054 (d, CH_3, 12H, J(H−H) 6.7 Hz), 2.10 (m, CH, 4H, J(H−H) 6.7 Hz), 1.49 (s, CH_3, 12H); group 2 1.13 (d, CH_3, 12H, J(H−H) 6.7 Hz), 1.11 (d, CH_3, 12H, J(H−H) 6.7 Hz), 2.04 (m, CH, 4H, J(H−H) 6.7 Hz), 1.51 (s, CH_3, 12H); group 3 1.10 (d, CH_3, 12H, J(H−H) 6.7 Hz), 2.06 (m, CH, 2H, J(H−H) 6.7 Hz), 1.53 (s, CH_3, 6H). Anal. Calcd for $Au_{10}C_{70}H_{110}O_{10}$: C, 27.29; H, 3.60. Found: C, 27.46; H, 3.62.

$(AuC_2C_6H_{13}O)_{10}$ (5). Pale yellow solid, poorly soluble in common organic solvents (89%). ES MS (m/z): $[M - H^+]^-$ 3219.6 (calcd 3219.6). The solubility of the complex in deuterated solvents was too low to obtain interpretable NMR data. Anal. Calcd for $Au_{10}C_{80}H_{130}O_{10}$: C, 29.83; H, 4.07. Found: C, 29.75; H, 4.10.

$(AuC_2C_6H_{11}O)_{10}$ (6). Lemon yellow powder, poorly soluble in common organic solvents (95%). ES MS (m/z): $[M - H^+]^-$ 3199.5 (calcd 3199.5). The solubility of the complex in deuterated solvents was too low to obtain interpretable NMR data. Anal. Calcd for $Au_{10}C_{80}H_{110}O_{10}$: C, 30.01; H, 3.46. Found: C, 30.22; H, 3.46.

$(AuC_2C_{10}H_{17}O)_{10}$ (7). Bright yellow solid, moderately soluble in common organic solvents (90%). ES MS (m/z): $[M - H^+]^-$ 3739.9 (calcd 3739.9). ^1H NMR (acetone-d_6, 298 K; δ): OH signals 4.35 (s, 4H), 4.02 (s, 2H), 3.94 (s, 4H); three groups of alkynyl ligands, group 1 0.88 (s, CH_3, 12H), 1.07 (s, CH_3, 12H), 1.10 (s, CH_3, 12H), 2.28 (ddd, CH_2, 4H, J(H−H) 13.3, 3.0, and 4.0 Hz), 2.23 (d, CH_2, 4H, J(H−H) 13.3 Hz), 1.71 (dd, CH, 4H, J(H−H) 4.0 and 4.0 Hz), 1.67 (m, CH_2, 4H, J(H−H) 13.0, 4.0, and 3.0 Hz), 1.68 (m, CH_2, 4H, J(H−H) 13.0, 12.0, and 4.0 Hz), 1.47 (m, CH_2, 8H, J(H−H) ca. 12.0 and 4.0 Hz); group 2 0.91 (s, CH_3, 12H), 1.11 (s, CH_3, 12H), 1.12 (s, CH_3, 12H), 2.35 (ddd, CH_2, 4H, J(H−H) 13.3, 3.0, and 4.0 Hz), 2.00 (d, CH_2, 4H, J(H−H) 13.3 Hz), 1.78 (dd, CH, 4H, J(H−H) 4.0 and 4.0 Hz), 1.71 (m, CH_2, 4H, J(H−H) 13.0, 12.0, and ~3.0 Hz), 1.53 (m, CH_2, 4H, J(H−H) ca. 13.0, 7.0, and 4.0 Hz), 2.15 (m, CH_2, 4H, J(H−H) ca. 12.0 and 4.0 Hz), 1.23 (m, CH_2, 4H, J(H−H) ca. 12.0 and 4.0 Hz); group 3 0.93 (s, CH_3, 6H), 1.13 (s, CH_3, 6H), 1.13 (s, CH_3, 6H), 2.38 (ddd, CH_2, 2H, J(H−H) 13.3, 3.0, and 4.0 Hz), 2.09 (d, CH_2, 2H, J(H−H) 13.3 Hz), 1.78 (dd, CH, 2H, J(H−H) 4.0 and 4.0 Hz), 1.72 (m, CH_2, 2H, J(H−H) 13.0, 12.0, and ~3.0 Hz), 1.52 (m, CH_2, 2H, J(H−H) ca. 13.0, 7.0, and 4.0 Hz), 2.17 (m, CH_2, 2H, J(H−H) ca. 12.0 and 4.0 Hz), 1.23 (m, CH_2, 2H, J(H−H) ca. 12.0 and 4.0 Hz). Anal. Calcd for $Au_{10}C_{120}H_{170}O_{10}$: C, 38.51; H, 4.58. Found: C, 38.83; H, 4.64.

Synthesis of $[Au_8(C_2R)_6(1,4\text{-}PPh_2C_6H_4PPh_2)_2]^{2+}$ Complexes 8−14. $(AuC_2R)_{10}$ (0.03 mmol) was dissolved/suspended in dichloromethane (8 cm^3), and $[Au_2(PPh_2C_6H_4PPh_2)_2]^{2+}$ (0.052 mmol) was added followed by acetone (5 cm^3). The reaction mixture was stirred overnight in the absence of light. The resulting transparent yellow solution was filtered and evaporated. Recrystallization of the crude material afforded complounds **8**−**14** as yellow crystalline solids.

$[Au_8(C_2C_{13}H_9O)_6(PPh_2C_6H_4PPh_2)_2](ClO_4)_2$ (8). Bright yellow powder (81%). ES MS (m/z): $[Au_8(C_2C_{13}H_9O)_6(PPh_2C_6H_4PPh_2)_2]^{2+}$ 1849.2 (calcd 1849.2). $^{31}P\{^1H\}$ NMR (acetone-d_6, 298 K; δ): 32.1 (s).

dx.doi.org/10.1021/ic300856h | *Inorg. Chem.* 2012, 51, 7392−7403

^{1}H NMR (acetone-d_6, 298 K; δ): diphosphine 7.81 (t, *para*-H Ph−P, 8H, J(H−H) ca. 7.0 Hz), 7.75 (dd, *meta*-H Ph−P, 16H, J(H−H) ca. 7.0 Hz), 7.52 (br m, *ortho*-H Ph−P, 16H), 6.29 (m AA′XX′, P−C_6H_4−P, 8H, J(H−H) ca. 7.5, J(P−H) ca. 14 Hz, J(P−P) ca. 30 Hz); two groups of alkynyl ligands {P−$AuC_2C_{13}H_9O$} fragments 5.99 (s, O*H*, 2H), 7.91 (d, 4H, J(H−H) av 7.5 Hz), 7.62 (d, 4H, J(P−H) 7.5 Hz), 7.42 (dd, 4H, J(H−H) 7.5 Hz), 7.04 (dd, 4H, J(H−H) 7.5 Hz); {$Au(C_2C_{13}H_9O)_2$} "rods" 5.79 (s, O*H*, 4H) 7.89 (d, 8H, J(H−H) av. 7.5 Hz), 7.18 (d, 8H, J(P−H) 7.5 Hz), 7.15 (dd, 8H, J(H−H) 7.5 Hz), 6.79 (dd, 8H, J(H−H) 7.5 Hz). Anal. Calcd for $Au_8C_{150}H_{102}Cl_2O_{14}P_4$: C, 46.21; H, 2.64. Found: C, 46.17; H, 2.60.

$[Au_8(C_2C_{13}H_{11}O)_6(PPh_2C_6H_4PPh_2)_2](PF_6)_2$ (9). Yellow block crystals (95%). ES MS (m/z): $[Au_8(C_2C_{13}H_{11}O)_6(PPh_2C_6H_4PPh_2)_2]^{2+}$ 1855.3 (calcd 1855.2). ^{31}P{^{1}H} NMR (acetone-d_6, 298 K; δ): 34.2 (s, 4P), −144.8 (sept, $2PF_6$). ^{1}H NMR (acetone-d_6, 298 K; δ): diphosphine 7.68 (t, *para*-H Ph−P, 8H, J(H−H) 7.6 Hz), 7.56 (dd, *ortho*-H Ph−P, 16H, J(H−H) 7.6 Hz, J(P−H) 14 Hz), 7.43 (dd, *meta*-H Ph−P, 16H, J(H−H) 7.6 Hz), 6.38 (m AA′XX′, P−C_6H_4−P, 8H, J(H−H) ca. 7.6, J(P−H) ca. 14 Hz, J(P−P) ca. 30 Hz); two groups of alkynyl ligands, {P−$AuC_2C_{13}H_{11}O$} fragments 6.63 (s, O*H*, 2H), 7.83 (m, *ortho*-H, 8H, J(H−H) ca. 7.6 Hz), 7.18−7.27 (AB system of *meta-para*-H, 12H, J(P−H) 7.6 Hz); {$Au(C_2C(OH)Ph_2)_2$} "rods" 6.03 (s, O*H*, 4H) 7.53 (d, *ortho*-H, 16H, J(H−H) ca. 7.9 Hz), 7.09 (t, *para*-H, 8H, J(P−H) 7.3 Hz), 6.95 (dd, *meta*-H, 16H, J(H−H) av. 7.6 Hz). Anal. Calcd for $Au_8C_{150}H_{114}F_{12}O_6P_6$: C, 45.02; H, 2.87. Found: C, 45.27; H, 3.07.

$[Au_8(C_2C_9H_{19}O)_6(PPh_2C_6H_4PPh_2)_2](PF_6)_2$ (10). Yellow crystals (89%). ES MS (m/z): $[Au_8(C_2C_9H_{19}O)_6(PPh_2C_6H_4PPh_2)_2]^{2+}$ 1735.5 (calcd 1735.4). ^{31}P{^{1}H} NMR (acetone-d_6, 298 K; δ): three signals at 34.9, 34.6, 32.9 ppm of total intensity 4, −144.8 (sept, $2PF_6$). ^{1}H NMR (acetone-d_6, 298 K; δ): major isomer (∼40%), diphosphine 7.94 (dd, *ortho*-H Ph−P, 16H, J(H−H) 7.5 Hz, J(P−H) 13.5 Hz), poorly resolved multiplets 7.50−7.77 (dd, *meta*-H Ph−P, 16H, J(H−H) ca. 7.5 Hz; t, *para*-H Ph−P, 8H, J(H−H) ca. 7.5 Hz; m AA′XX′, P−C_6H_4−P, 8H, J(H−H) ca. 7.5, J(P−H) ca. 14 Hz); two groups of alkynyl ligands (COSY-DQF spectrum was used for signals assignment), {P−$AuC_2C_9H_{19}O$} fragments 4.62 (s, O*H*, 2H), 0.909 (d, CH_3, 12H, J(H−H) 6.7 Hz), 0.882 (d, CH_3, 12H, J(H−H) 6.7 Hz), 1.981 (m, CH, 4H, J(H−H) 6.7, 5.2, and 6.4 Hz), 1.648 (dd, CH_2, 4H, J(H−H) 14.0 and 6.4 Hz), 1.661 (dd, CH_2, 4H, J(H−H) 14.0 and 5.2 Hz); {$Au(C_2C_9H_{19}O)_2$} "rods" 4.34 (s, O*H*, 4H), 0.86 (d, CH_3, 24H, J(H−H) 6.7 Hz), 0.83 (d, CH_3, 24H, J(H−H) 6.7 Hz), 1.898 (m, CH, 8H, J(H−H) 6.7, 6.4, and 6.4 Hz), 1.679 (d, CH_2, 16H, J(H−H) 6.4 Hz). A few minor isomers, diphosphine unresolved multiplets 7.50−7.77 (dd, *ortho*-H Ph−P, 16H, J(H−H) 7.5 Hz, J(P−H) 13.5 Hz; dd, *meta*-H Ph−P, 16H, J(H−H) ca. 7.5 Hz; t, *para*-H Ph−P, 8H, J(H−H) ca. 7.5 Hz; m AA′XX′ 8H, P−C_6H_4−P, J(H−H) ca. 7.5, J(P−H) ca. 14 Hz); OH signals 4.78, 4.65, and 4.61 (s, ca. 2H), 4.40, 4.38, and 4.33 (s, ca. 4H); two groups of alkynyl ligands unresolved multiplets 0.90−1.05 (d, CH_3, 72H, J(H−H) 6.7 Hz), unresolved multiplets 1.95−2.27 (m, CH, 12H, J(H−H) ca. 6.7, 5.2, and 6.4 Hz), unresolved multiplets 1.64−1.95 (dd, CH_2, 12H, J(H−H) 14.0 and 5.2 Hz; dd, CH_2, 12H, J(H−H) 14.0 and 6.4 Hz). A slow exchange between the isomers was revealed due to exchange cross-peaks in the NOESY spectrum. Anal. Calcd for $Au_8C_{126}H_{162}F_{12}O_6P_6$: C, 40.23; H, 4.34. Found: C, 40.35; H, 4.46.

$[Au_8(C_2C_5H_{11}O)_6(PPh_2C_6H_4PPh_2)_2](PF_6)_2$ (11). Yellow block crystals (91%). ES MS (m/z): $[Au_8(C_2C_5H_{11}O)_6(PPh_2C_6H_4PPh_2)_2]^{2+}$ 1567.3 (calcd 1567.2). ^{31}P{^{1}H} NMR (acetone-d_6, 298 K; δ): 8 broadened signals in the interval 33−36 ppm of total intensity 4, −144.8 (sept, $2PF_6$). ^{1}H NMR (acetone-d_6, 298 K; δ) corresponds to a mixture of more than four isomers with slow chemical exchange between them observed in the EXSY-NOESY spectrum: diphosphine unresolved multiplets, 7.81−8.07 (dd, *ortho*-H Ph−P, 16H all isomers), 7.45−7.77 (dd, *meta/para*-H Ph−-P, 16H all isomers; m, AA′XX′, P−C_6H_4−P, 8H all isomers); two groups of alkynyl ligands with the cross-peaks found in COSY-DQF and NOESY spectra inside each of the groups: OH signals two sets of singlets 4.91−4.94 (2H), 4.39−4.48 (s, 4H); {P−Au−$C_2C_5H_{11}O$} fragments poorly resolved multiplets at 1.10−1.19 (d, CH_3, 12H all isomers, J(H−H) 6.7 Hz), 2.08−2.21 (m, CH, 2H all isomers, J(H−H) 6.7 Hz), 1.62−1.69 (s, CH_3, 6H all isomers); {Au−$(C_2C_5H_{11}O)_2$} "rods" poorly resolved multiplets at 1.01−1.13 (d, CH_3, 24H all isomers, J(H−H) 6.7 Hz), 1.86−2.00 (m, CH, 4H all isomers, J(H−H) 6.7 Hz), 1.31−1.42 (s, CH_3, 12H all isomers). Anal. Calcd for $Au_8C_{102}H_{114}F_{12}O_6P_6$: C, 35.76.23; H, 3.35. Found: C, 35.87; H, 3.35.

$[Au_8(C_2C_6H_{13}O)_6(PPh_2C_6H_4PPh_2)_2](PF_6)_2$ (12). Yellow block crystals (90%). ES MS (m/z): $[Au_8(C_2C_6H_{13}O)_6(PPh_2C_6H_4PPh_2)_2]^{2+}$ 1609.3 (calcd 1609.3). ^{31}P{^{1}H} NMR (acetone-d_6, 298 K; δ): 12 broadened signals in the interval 33.5−35.5 ppm of total intensity 4, −144.8 (sept, $2PF_6$). ^{1}H NMR (acetone-d_6, 298 K; δ) corresponds to a mixture of the isomers under the condition of slow exchange: diphosphine unresolved multiplets 7.80−8.08 (dd, *ortho*-H Ph−P, 16H all isomers), 7.46−7.78 (dd, *meta/para*-H Ph−P, 24H all isomers; m, AA′XX′, P−C_6H_4−P, 8H all isomers); OH signals 4.88−5.06 (s, 2H), 4.49−4.58 (s, 4H); two groups of alkynyl ligands with the relative intensity 2/1 related by the cross-peaks in the COSY-DQF and NOESY spectra inside each of the groups: {P−Au−$C_2C_6H_{13}O$} fragments poorly resolved multiplets 0.93−1.04 (d, CH_3, 6H all isomers, J(H−H) 6.7 Hz), 2.02−2.24 (m, CH, 2H all isomers, J(H−H) 6.7 Hz), 1.76−1.91 (dd, CH_2, 4H all isomers, J(H−H) 14.0 and ca. 6.4 Hz), 1.66−1.81 (s, CH_3, 6H all isomers); {Au−$(C_2C_6H_{13}O)_2$} "rods" poorly resolved multiplets 0.85−0.97 (d, CH_3, 24H all isomers, J(H−H) 6.7 Hz), 1.93−2.14 (m, CH, 4H all isomers, J(H−H) 6.7 Hz), 1.65−1.73 (dd, CH_2, 8H all isomers, J(H−H) 14.0 and ca. 6.4 Hz), 1.40−1.54 (s, CH_3, 12H all isomers). Anal. Calcd for $Au_8C_{108}H_{126}F_{12}O_6P_6$: C, 36.96.23; H, 3.62. Found: C, 37.09; H, 3.43.

$[Au_8(C_2C_6H_{11}O)_6(PPh_2C_6H_4PPh_2)_2](PF_6)_2$ (13). Yellow block crystals (94%). ES MS (m/z): $[Au_8(C_2C_6H_{11}O)_6(PPh_2C_6H_4PPh_2)_2]^{2+}$ 1603.3 (calcd 1603.2). ^{31}P{^{1}H} NMR (acetone-d_6, 298 K; δ): three broadened signals in the interval 34−36 ppm of total intensity 4, −144.8 (sept, $2PF_6$). ^{1}H NMR (acetone-d_6, 298 K; δ): a set of unresolved multiplets in the aromatic area (7.4−8.6 ppm, diphosphine ligand), hydroxyl group singlets (4.6−5.6 ppm), and aliphatic radicals region (0.6−2.2 ppm) corresponding to the mixture of isomers under the condition of slow exchange. Anal. Calcd for $Au_8C_{108}H_{114}F_{12}O_6P_6$: C, 37.09; H, 3.29. Found: C, 37.17; H, 3.21.

$[Au_8(C_2C_{10}H_{17}O)_6(PPh_2C_6H_4PPh_2)_2](PF_6)_2$ (14). Yellow block crystals (93%). ES MS (m/z): $[Au_8(C_2C_{10}H_{17}O)_6(PPh_2C_6H_4PPh_2)_2]^{2+}$ 1765.4 (calcd 1765.4). ^{31}P{^{1}H} NMR (acetone-d_6, 298 K; δ): 34.2 (s, 4P), −144.8 (sept, $2PF_6$). ^{1}H NMR (acetone-d_6, 298 K; δ): diphosphine 7.95 (*ortho*-H, complex multiplet due to coupling to the A_2B system of the *meta-para* protons, 16H), 7.54−7.76 (unresolved multiplets due to A_2B system of the *meta-para* protons, (16 + 8) H, and AA′XX′ system of (P−C_6H_4−P), 8H); two groups of alkynyl ligands (COSY and NOESY spectra were used for signals assignment) {P−$AuC_2C_{10}H_{17}O$} fragments: 4.81 (s, O*H*, 2H), 0.89 (s, CH_3, 6H), 0.86 (s, CH_3, 6H), 1.08 (s, CH_3, 6H), 2.51 (ddd, CH_2, 2H, J(H−H) 13.3, 3.0, and 4.0 Hz), 2.19 (d, CH_2, 2H, J(H−H) 13.3 Hz), 1.83 (dd, CH, 2H, J(H−H) 4.0 and 4.0 Hz), 1.55 (m, CH_2, 2H, J(H−H) 13.0, 12.0, and ∼3.0 Hz), 2.11 (m, CH_2, 2H, J(H−H) ca. 13.0, 7.0, and 4.0 Hz), 1.28 (m, CH_2, 4H, J(H−H) ca. 12.0 and 4.0 Hz); {$Au(C_2C_{10}H_{17}O)_2$} "rods" 4.28 (s, O*H*, 4H), 0.842 (s, CH_3, 12H), 0.802 (s, CH_3, 12H), 1.015 (s, CH_3, 12H), 2.298 (ddd, CH_2, 4H, J(H−H) 13.3, 3.0, and 4.0 Hz), 1.963 (d, CH_2, 4H, J(H−H) 13.3 Hz), 1.758 (dd, CH, 4H, J(H−H) 4.0 and 4.0 Hz), 1.61 (m, CH_2, 4H, J(H−H) 13.0, 4.0, and 3.0 Hz), 1.216 (m, CH_2, 4H, J(H−H) 13.0, 12.0, and 4.0 Hz), 1.263 (m, CH_2, 8H, J(H−H) ca. 12.0 and 4.0 Hz). Anal. Calcd for $Au_8C_{132}H_{150}F_{12}O_6P_6$: C, 41.48; H, 3.96. Found: C, 41.46; H, 4.09.

X-ray Structure Determination. Crystals of **1**, **13**, and **14** were immersed in cryo-oil, mounted in a Nylon loop, and measured at a temperature of 100 K. X-ray diffraction data were collected on a Bruker Kappa Apex II or Bruker Kappa Apex II Duo diffractometer using Mo Kα radiation (λ = 0.71073 Å). The *APEX2*[13]program package was used for cell refinements and data reduction. Structures were solved by direct methods using the *SHELXS-97*[14] and *SUPERFLIP*[15] programs with the *WinGX*[16] graphical user interface. A semiempirical absorption correction (*SADABS*)[17] was applied to all data. Structural refinements were carried out using *SHELXL-97*.[14] Some of the solvent molecules in the crystals of **1** and **13** were omitted as they were disordered and could not been resolved unambiguously. The missing solvent was taken into account using a *SQUEEZE* routine of *PLATON*.[18] The contribution of

dx.doi.org/10.1021/ic300856h | *Inorg. Chem.* 2012, 51, 7392−7403

Scheme 1. Synthesis of Complexes 1−7[a]

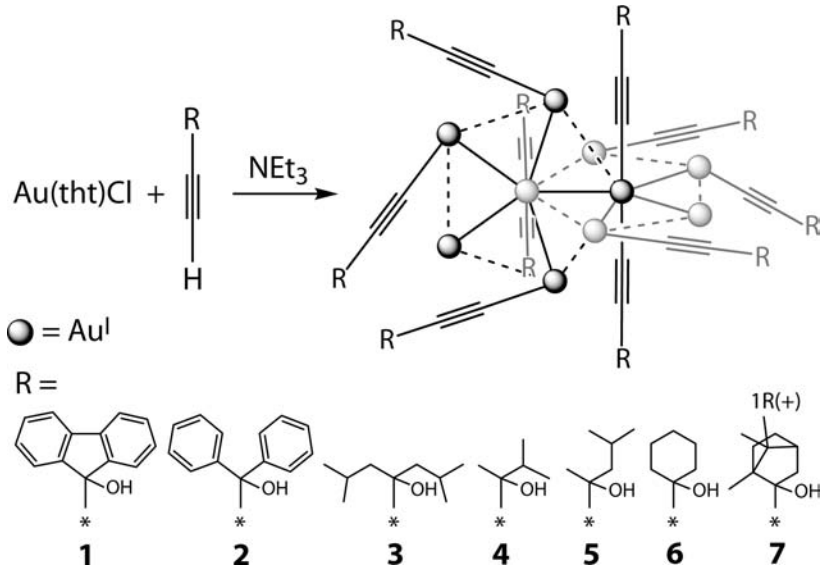

[a]Acetone, 0.5 h, 298 K, yields 81−95%.

the solvent to the cell content was not taken into account. Two of the resolved ethanol molecules in **1** were refined with occupation factor 0.5. One of the aromatic moieties was slightly disordered. However, no disorder model was used during the final refinement. The aromatic rings C139−C144 and C145−C150 were geometrically idealized. These carbon atoms as well as C107, C137, and C139−C151 and solvent oxygens were restrained, so that their U_{ij} components approximate isotropic behavior. The crystal of **13** was refined as a racemic twin. The absolute structure parameter was refined to 0.056(19). The C−C distances in the cyclohexyl groups C41−C46 and C48−C53 in **13** were restrained to be similar as well as the P−F and F−F distances in one of the PF_6^- counteranions. The fluorine atoms F7−F12 as well as carbon atoms C33, C39, C40, and C54 were restrained so that its U_{ij} components approximate isotropic behavior. In **14** one of the acetone solvent molecules was partially lost and refined with an occupancy of 0.5. Idealized positions of the OH hydrogens for oxygen atoms O1−O5 were estimated with the *HYDROGEN*[19] program and constrained to ride on their parent atom with U_{iso} = 1.5 (parent atom). The OH hydrogen of O6 was positioned manually and constrained to ride on its parent atom. Other hydrogen atoms in all structures were positioned geometrically and constrained to ride on their parent atoms, with C−H = 0.95−0.99 Å, O−H 0.84 Å, U_{iso} = 1.2−1.5U_{eq} (parent atom). Crystallographic details are summarized in Table S1, Supporting Information.

Photophysical Measurements. Steady-state absorption and emission measurements were recorded on a Hitachi (U-3310) spectrophotometer and an Edinburgh (FS920) fluorometer, respectively. Both the wavelength-dependent excitation and the emission response of the fluorometer have been calibrated. To determine the photoluminescence quantum yield in solution, the samples were degassed by three freeze−pump−thaw cycles. 4-(Dicyanomethylene)-2-methyl-6-(paradimethylaminostyryl)-4Hpyran (DCM, λ_{max} = 615 nm, Exciton) in methanol and coumarin 480 in methanol, with quantum yields of 0.4 and 0.87, respectively, were used as the standards for the quantum yield measurements. Steady-state emission measurements in the solid state were measured by an Edinburgh (FS920) fluorometer. Photoluminescence quantum yields in the solid state were determined with a calibrated integrating sphere system (HAMAMATSU C9920). The PLQY measurements were conducted in solid films prepared on a quartz plate (1.6 × 1.0 cm^2). Quantum efficiency measurements were recorded with an integration sphere coupled with a photonic multichannel analyzer C10027 (HAMAMATSU), which gave the reference anthracene a quantum yield of 23%. The uncertainty of the quantum yield measurement was in the range of <2% (an average of four replica). Lifetime studies were performed with an Edinburgh FL 900 photon-counting system using a hydrogen-filled lamp as the excitation source. Emission decays were fitted by the sum of exponential functions with a temporal resolution of 300 ps by deconvolution of the instrument response function.

Computational Details. The Au^I_{10} clusters **1**−**7** and Au^I_8 clusters **8**−**14** were studied using the hybrid PBE0 density functional.[20] The gold atoms were described by a triple-valence zeta-quality basis set with polarization functions (def2-TZVP).[21] Scalar relativistic effects were taken into account by employing a 60-electron relativistic effective core potential for gold.[22] A split-valence basis set with polarization functions on non-hydrogen atoms was used for the other atoms.[23] The multipole-accelerated resolution of the identity technique was used to speed up the calculations.[24] The excited states were investigated with the time-dependent DFT approach.[25] To facilitate comparisons with the experiments, point group symmetry was applied where possible (the point group symmetry of complexes **1**−**7** and **8**−**14** had to be lowered from the experimentally observed ideal D_{2d} and D_{2h} as the flexible rotation of the alkynyl ligands cannot be described by the calculations). All electronic structure calculations were carried out with the TURBOMOLE program package (version 6.3).[26]

RESULTS AND DISCUSSION

Preparation of the homoleptic alkynyl compounds $(AuC_2R)_n$ (R = aromatic or aliphatic group) generally involves treatment of the labile complex LAuCl (L = dimethylsulfide, tetrahydrothiophene) with a stoichiometric amount of the alkyne and base ($NaOOCCH_3$, amine), resulting in poorly soluble polymeric materials.[6a,b,27] When the hydroxyaliphatic alkynes HC_2R (R = −C(OH)R′$_2$) were employed in this synthetic procedure, bright yellow complexes identified as decanuclear clusters $(AuC_2R)_{10}$ were obtained in high yields (Scheme 1).

Compounds **1**−**7** were studied by ^{1}H spectroscopy and ESI-MS. The solid-state structure of **1** was determined by an X-ray diffraction study (Figure 2). The molecule consists of two fused, nearly planar Au_5 pentagons, which are roughly perpendicular to each other. Alternatively, it may be considered as a catenane structure with two interlocked 5-membered rings: a smaller congener of the bis-hexagonal $[(AuC_2{-}Bu^t)_6]_2$ complex.[5a] The unprecedented decametallic core is held together by Au−Au and π-C≡C−Au interactions. The intermetallic distances range

dx.doi.org/10.1021/ic300856h | Inorg. Chem. 2012, 51, 7392−7403

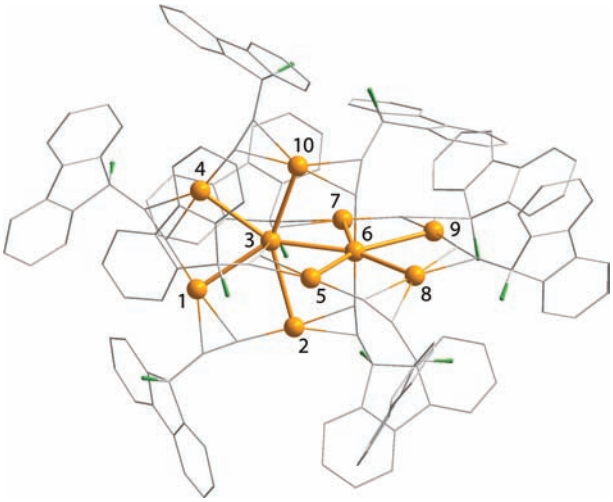

Figure 2. Molecular view of complex **1**: yellow, gold; green, oxygen. Selected interatomic distances (Å): Au(1)−Au(3) 3.0062(5), Au(2)−Au(3) 3.0661(6), Au(3)−Au(6) 2.9130(5), Au(3)−Au(10) 2.9606(5), Au(3)−Au(4) 2.9766(5), Au(5)−Au(6) 3.0537(5), Au(6)−Au(7) 3.0937(5), Au(6)−Au(8) 2.8804(5), Au(6)−Au(9) 3.0010(5).

from 2.8804(5) to 3.0937(5) Å. The former Au−Au bond length is very short and less than the Au−Au separation found in metallic gold (2.889 Å).[28] The values of gold−gold contacts (<3.1 Å) suggest the presence of extensive aurophilic interactions[5i] and are visibly shorter than those determined in the reported homoleptic alkynyl complexes $(AuC_2R)_n$ (2.98−3.36 Å).[5a−c]

The composition of **1** was confirmed by ESI-MS measurements in the negative mode, which display a dominating signal of the singly charged anion at m/z 4019.4 (Figure S1, Supporting Information), corresponding to the deprotonated form $[\mathbf{1} - H^+]^-$. The observed isotopic pattern fits completely the proposed stoichiometry.

Complexes **2**−**7** did not give crystals suitable for the X-ray diffraction study and were characterized by spectroscopic methods. Their ESI-MS are similar to that of **1** and show signals of the corresponding molecular ions at m/z 4039.5, 3640.1, 3079.5, 3219.6, 3199.5, and 3739.9, matching the composition of the deprotonated clusters (Figure S1, Supporting Information).

The 1D ^{1}H and multipulse (COSY, DQF COSY, J-COSY, HSQC, and NOESY) NMR measurements for **1**−**4** and **7** showed that the structure found in the solid state remains unchanged in solution (**5** and **6** could not be properly analyzed due to their very low solubility in deuterated solvents). Proton spectra of these complexes display three groups of signals with relative intensities 4:4:2 (see Experimental Section and Figures 3 and S2−S6, Supporting Information), which are particularly visible in the area typical for the hydroxyl protons (5.0−6.5 ppm for **1** and **2**, 4.0−5.0 for **3** and **4**, **7**). Analogous grouping of the resonances corresponding to the aromatic (**1** and **2**) and aliphatic alkynyl substituents (**3**, **4**, **7**) was observed in the low- and high-field parts of the spectra. Within every group, all signals were related to each other as determined in ^{1}H−^{1}H COSY experiments.

The latter observation was additionally supported by the data of J-COSY (Figure S3, Supporting Information) and NOESY spectra. Relative intensities (4:4:2) of these groups of resonances fit completely the structural pattern shown in Scheme 1 and Figure 2, where two rings are naturally equivalent and fast dynamics (semibridging ↔ terminal alkynyls) results in the D_{2d} point symmetry group of the idealized molecule, where 2-fold axes go along and perpendicular to the Au(3)−Au(6) bond (Figure 2), while each Au_5 pentagon lies in one of the mirror planes. This makes the alkynyl ligands equivalent at Au(3), Au(6) and Au(2), Au(10), Au(7), Au(5) ions to give two sets of resonances of quadruple intensity, whereas the set of double-intensity signals should be assigned to the substituent of the alkynyl ligands bridging Au(1)/Au(4) and Au(8)/Au(9) ion pairs. Interestingly, in the case of **1**, a set of signals of a minor form was detected, the concentration of which increases upon dilution of the complex solutions (Figure 4). The process is completely reversible, and the minor form can be suppressed by raising the solution concentration.

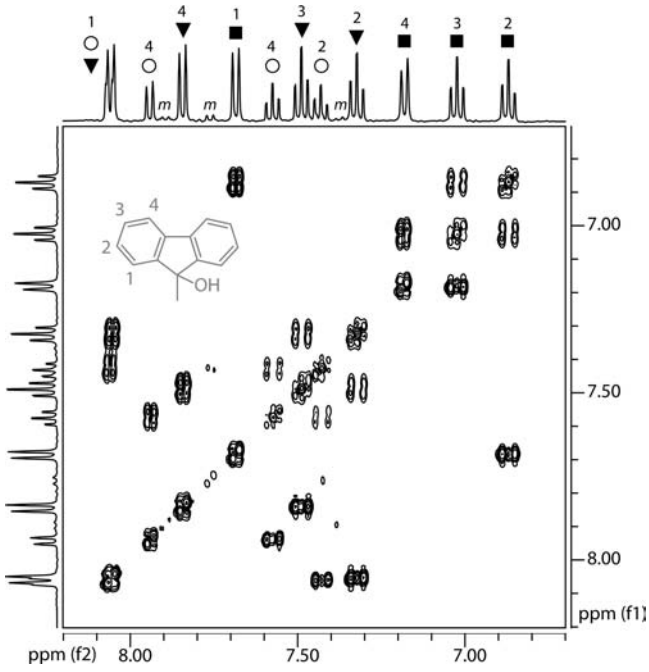

Figure 3. ^{1}H−^{1}H COSY spectrum of the major form of **1**, aromatic region, acetone-d_6, 298 K: (▼, ■, ○) signals of three groups of the alkynyl ligands; signals of the fluorenol moiety protons are numbered as schematically shown in the figure; (m) signals of the minor form of **1**.

Four signals of the minor component of **1** can be easily assigned to the protons of the fluorenol group of the alkynyl ligand similarly to the major form (Figure 3, see Experimental Section), which is indicative of a structural pattern with all-equivalent alkynyl groups. These observations point to a chemical equilibrium, which on dilution probably results in formation of a symmetrical tetragold cluster (Scheme 2). The latter might display a structural motif found earlier for the complex containing alkynylcalix[4]crown-6 ligand.[5b] Integration of the spectrum corresponding to the dilute solution shows that the major and minor forms exist in approximately equivalent quantities provided that the components adopt the structures depicted in Scheme 2.

In our recent communication, we reported the synthesis of octanuclear gold clusters via treatment of $(AuC_2R)_n$ (R = Bu^t) with a stoichiometric amount of digold−diphosphine complexes $[Au_2(PPh_2-X-PPh_2)_2]^{2+}$ (X = −C≡C−, $-C_6H_4-$).[5f] The same approach was applied for compounds **1**−**7**, allowing effective isolation of a family of $[Au_8(C_2R)_6(1,4\text{-}PPh_2C_6H_4PPh_2)_2]^{2+}$ (**8**−**14**) clusters as yellow crystalline solids (Scheme 3).

dx.doi.org/10.1021/ic300856h | Inorg. Chem. 2012, 51, 7392−7403

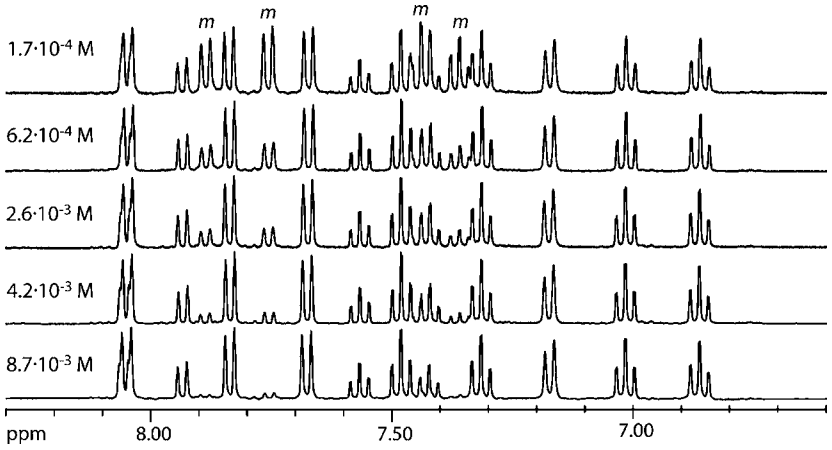

Figure 4. ^{1}H NMR spectra of **1** at different concentrations, aromatic region, acetone-d_6, 298 K; *m* denotes signals of the minor form. Further dilution did not change the ratio of the two forms. Higher concentrations were not accessible due to the solubility limit.

Scheme 2. Proposed Equilibrium for Cluster 1 in Solution

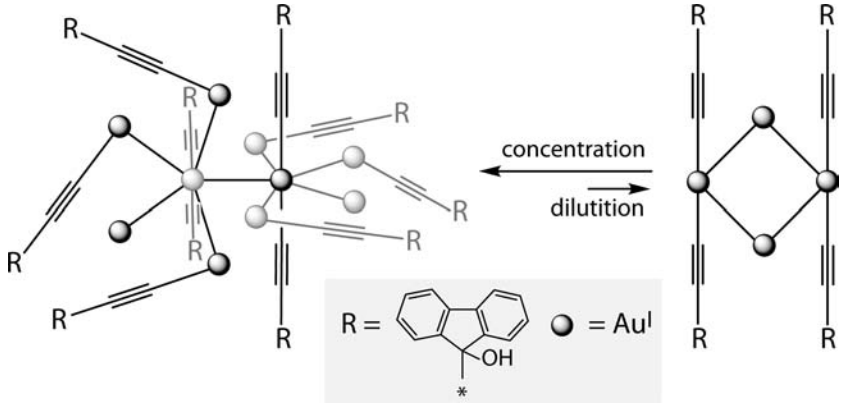

Scheme 3. Synthesis of Complexes 8−14[a]

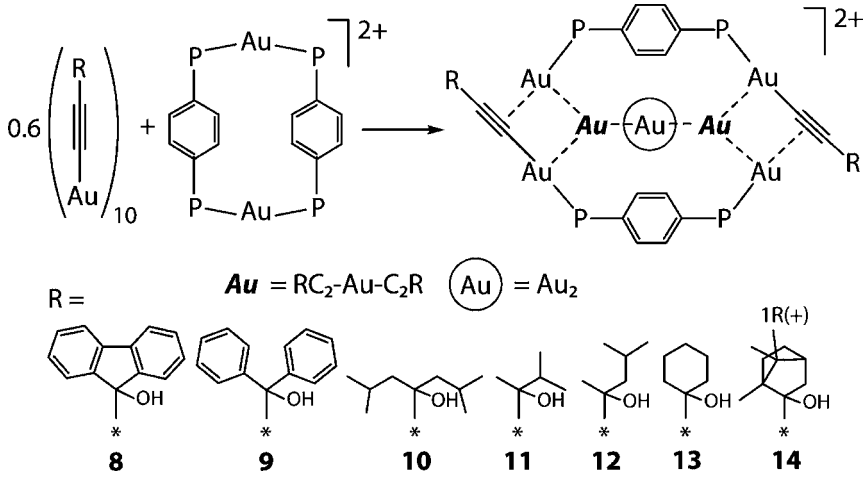

[a]Acetone/dichloromethane mixture, overnight, 298 K, yields 81−95%.

Clusters **8**−**14** were studied by ^{1}H and ^{31}P NMR spectroscopy and ESI-MS. The solid-state structures of **13** and **14** were determined by X-ray diffraction analysis (Figure 5). The molecules consist of approximately planar tetranuclear $Au_4(C_2R)_4$ cluster cores, which are embedded in between two digold cationic units, formulated as $[Au(PPh_2C_6H_4PPh_2)Au(\eta^1{:}\eta^2\text{-}C_2R)]^+$ (Scheme 3). These fragments are held together by the Au−Au interactions and π-C≡C−Au bonding. This structural pattern is exactly the same as that found earlier for the $[Au_8(C_2R)_6(1,4\text{-}PPh_2C_6H_4PPh_2)_2]^{2+}$ (R = Bu^{t}) derivative,[5f] pointing to a negligible influence of the alkynyl substituents on the general motif of this type of clusters in the solid state.

The central tetranuclear clusters in both **13** and **14** are slightly asymmetric, having two short Au−Au distances (3.0998(8)−

dx.doi.org/10.1021/ic300856h | Inorg. Chem. 2012, 51, 7392−7403

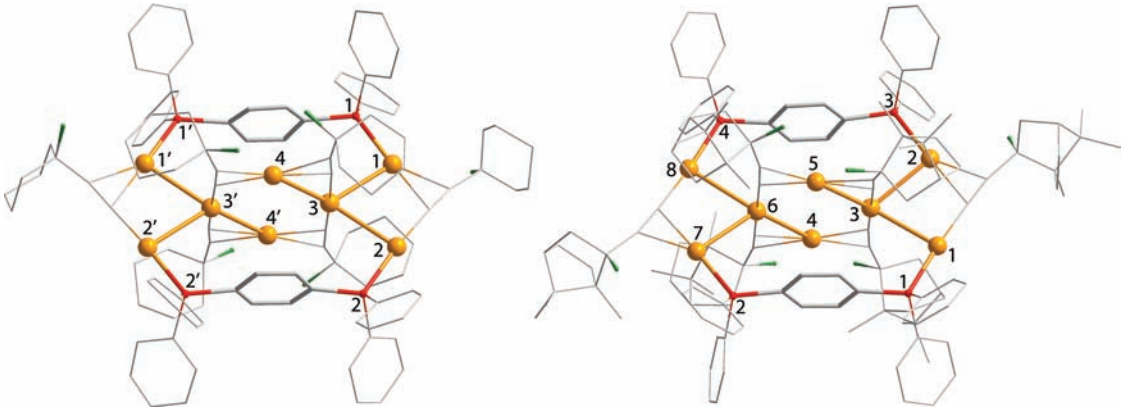

Figure 5. Molecular views of the dications **13** (left) and **14** (right): yellow, gold; red, phosphorus; green, oxygen. Selected interatomic distances (Å) in **13**: Au(1)−P(1) 2.267(5), Au(1)−Au(3) 2.8937(9), Au(2)−P(2) 2.289(4), Au(2)−Au(3) 2.9192(9), Au(3)−Au(4) 3.0998(8), Au(3)−Au(4′) 3.2834(8). Symmetry transformations used to generate equivalent atoms: $-x, y, -z + 1/2$. Selected interatomic distances (Å) in **14**: P(1)−Au(1) 2.2829(16), P(2)−Au(7) 2.2851(17), P(3)−Au(2) 2.2778(17), P(4)−Au(8) 2.2900(17), Au(1)−Au(3) 2.9672(4), Au(2)−Au(3) 2.8743(3), Au(3)−Au(5) 3.1185(4), Au(3)−Au(4) 3.2916(4), Au(4)−Au(6) 3.1455(4), Au(5)−Au(6) 3.2773(4), Au(6)−Au(7) 2.8911(3), Au(6)−Au(8) 2.9637(4).

3.1455(4) Å) and two elongated ones (3.2773(4)−3.2916(4) Å). All these contacts suggest the presence of attractive interactions as they are less than the sum of two Au van der Waals radii (3.32 Å). The metal−metal contacts between the central and the external fragments are generally shorter and do not exceed the value of 2.9637(4) Å, while the closest contact of 2.8743(3) Å (Au(2)−Au(3) in **14**) testifies to the significant interaction between the gold ions.

The ESI-MS of **8**, **9**, **10**, **11**, **12**, **13**, and **14** display the signals of doubly charged cations at m/z 1849.2, 1855.3, 1735.5, 1567.3, 1609.3, 1603.3, and 1765.4, respectively (Figure S7, Supporting Information). The isotopic patterns observed completely fit the stoichiometry of the corresponding $[Au_8(C_2R)_6(PPh_2C_6H_4PPh_2)_2]^{2+}$ molecular ions.

NMR characterization of the clusters **8**−**14** reveal that **8**, **9**, and **14** are structurally rigid and retain their structures in acetone-d_6 solution, while compounds **10**−**13** show complicated dynamic behavior. Complexes **8**, **9**, and **14** display single resonances in their ^{31}P spectra at 32.1, 34.2, and 34.2 ppm, respectively, that fall in the range typical for Au(I) coordinated tertiary arylphosphine. This observation indicates fast $\eta^1{:}\eta^2 \leftrightarrow \eta^2{:}\eta^1$ dynamics of the alkynyl groups of the external $[Au(PPh_2C_6H_4PPh_2)AuC_2R]^+$ fragments, resulting in the idealized D_{2h} molecular symmetry and making all phosphorus atoms equivalent. Proton NMR spectra of these complexes are also compatible with this structural hypothesis. In solution clusters **8** and **9** display spectroscopic patterns, which contain a low-field set of signals corresponding to the phenyl substituents at the phosphorus atoms and a characteristic AA′XX′ multiplet of the phenylene spacer in the high-field part of the spectrum (Figure 6). This complicated set of resonances is typical for the bridging (−Au−P−C_6H_4−P−Au−) coordination of the diphosphine ligand observed in the structurally related Au−Cu complexes.[8] The other signals detected in these spectra can be easily divided into two groups, as shown in Figure 6 and described in the Experimental Section, on the basis of the correlations observed in the $^1H-^1H$ COSY spectra, number, and relative intensities (1:2) of the corresponding groups of signals. These observations allow for assignment of these spectroscopic patterns to the aromatic substituents (well-resolved multiplets in the 6.7−8.0 ppm range) and hydroxyl protons (isolated singlets around 6 ppm) of the $\{P-AuC_2R\}$ fragments and the $\{Au(C_2R)_2\}$ rods.

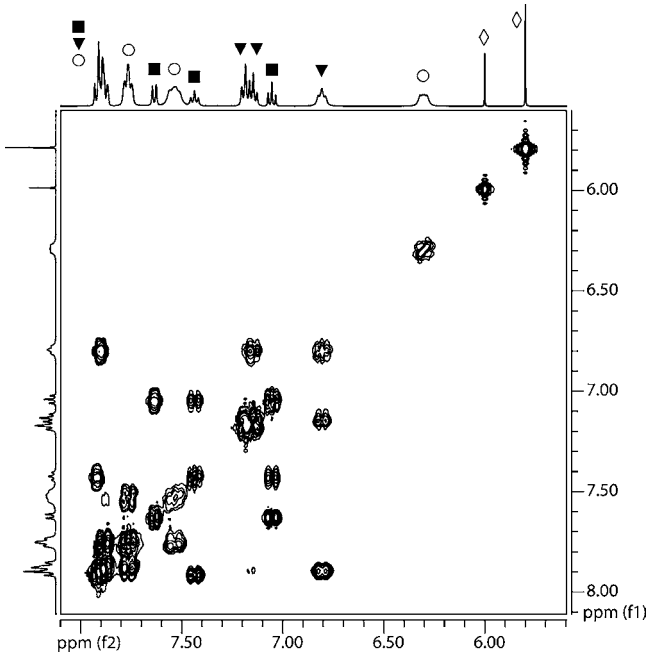

Figure 6. $^1H-^1H$ COSY spectrum of **8**, aromatic region, acetone-d_6, 298 K: (○) signals corresponding to diphosphine protons, (■) protons of the $\{P-Au(C_2C_{13}H_{11}O)\}$ fragments (▼) protons of the $[Au(C_2C_{13}H_{11}O)_2]^-$ rods, and (◇) OH groups.

^1H NMR data obtained for **14**, which bears aliphatic alkyne ligands derived from (1*R*)-(+)-camphor, are essentially similar, indicating the presence of only one molecular form in solution (Figures S8 and S9, Supporting Information). The spectrum contains a group of signals in the aromatic area, which can be easily assigned to the protons of the diphosphine ligands. Two singlets at 4.81 (2H) and 4.28 (4H) correspond to the hydroxyl protons, whereas multiplets in the aliphatic area can be also separated into two well-resolved (in the COSY and NOESY spectra) groups of resonances arising from the protons of the alkynyl substituents in the $\{Au(C_2R)_2\}$ rods and the $\{P-AuC_2R\}$ fragments.

In the case of clusters **10**−**13** containing alkynyl ligands with other aliphatic substituents (Scheme 3), spectroscopic data revealed the presence of at least several isomers, very probably

dx.doi.org/10.1021/ic300856h | *Inorg. Chem.* 2012, 51, 7392−7403

Scheme 4. Proposed Interconversion between Two Structural Types in the Titled Au_8 Complexes

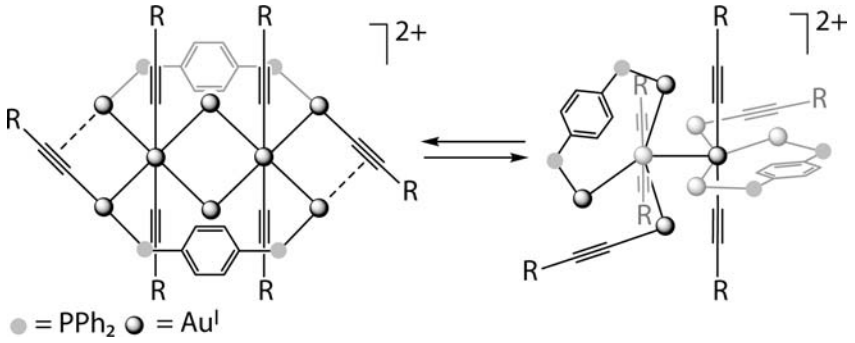

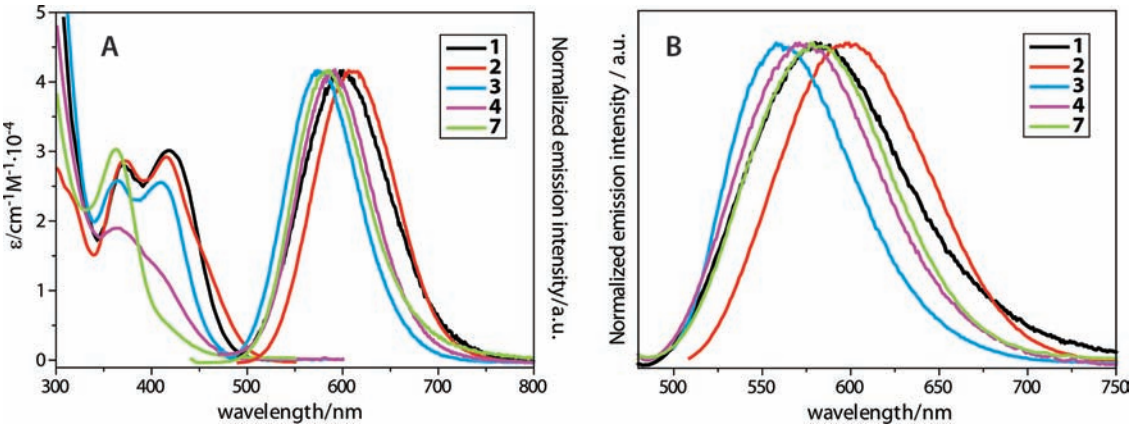

Figure 7. (A) UV−vis absorption and normalized emission spectra of **1**−**4** and **7** in aerated CH_2Cl_2 (298 K, λ_{ex} = 430 nm). (B) Normalized emission spectra of **1**−**4** and **7** in the solid state (298 K, λ_{ex} = 470 nm).

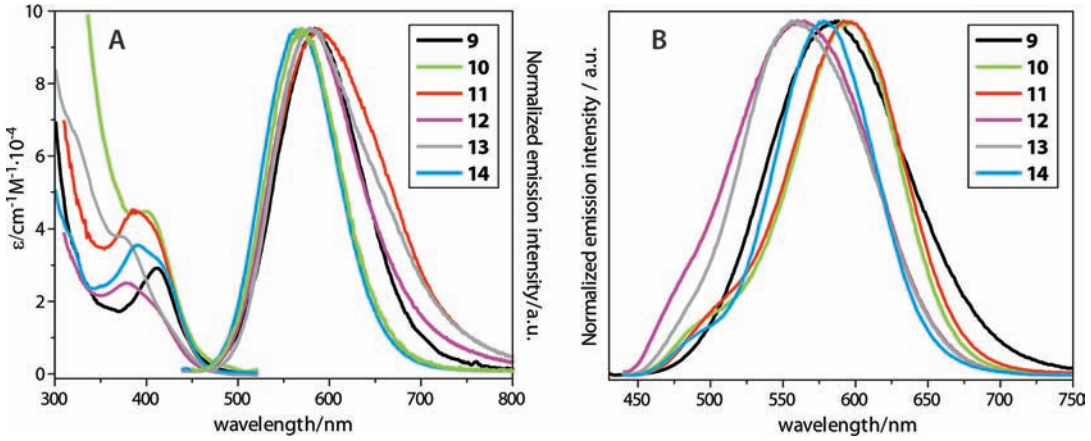

Figure 8. (A) UV−vis absorption and normalized emission spectra of **9**−**14** in aerated CH_2Cl_2 (298 K, λ_{ex} = 430 nm). (B) Normalized emission spectra of **9**−**14** in the solid state (298 K, λ_{ex} = 430 nm).

arising from the different orientation of the bulky aliphatic substituents inside the central core. Additionally, possible exchange between two structural types previously described for the octanuclear gold complexes[5f] can be taken into consideration (Scheme 4). The computational results (see below) show that these two configurations are energetically very close to each other for clusters **10**−**13**, enabling the dynamics observed in solution. This process does not require a change of the stoichiometry and therefore is in line with mass-spectroscopic measurements, which showed dominant signals of the $[Au_8(C_2R)_6(PPh_2C_6H_4PPh_2)_2]^{2+}$ dications for all octanuclear compounds **8**−**14** (Figure S7, Supporting Information), indicating that these clusters do not demonstrate a significant tendency to dissociate into smaller fragments. The presence of several components in solutions of **10**−**13**, together with slow and complex exchange dynamics resulting in substantial broadening of the signals both in the ^{31}P and ^{1}H spectra, make these spectroscopic patterns poorly resolved and extremely complicated.

Photophysical Results. Figures 7 and 8 show the UV−vis absorption and normalized emission spectra for **1**−**4** and **7** and **9**−**14** in CH_2Cl_2, respectively. Complexes **5** and **6** are not included due to their sparse solubility in common organic solvents. Also, complex **8** undergoes certain unknown photo-

dx.doi.org/10.1021/ic300856h | Inorg. Chem. 2012, 51, 7392−7403

decomposition in CH_2Cl_2 and hence will not be discussed here to avoid complexity.

Evidently, the electronic absorption spectra of all octanuclear complexes are characterized by two major absorption bands at <340 and 340−500 nm. Following the assignment of the previous reports,[8] the absorption below 340 nm can be ascribed to the electronic transition from the σ(Au−P) orbital to an empty π^* (C≡C) antibonding orbital located at the alkynyl ligand. As shown in the computational section, the lower lying absorption bands of all studied complexes (340−500 nm) are related to a metal-centered Au−Au transition mixed, in part, with a transfer of electron density from the metal (Au) to the ligand (alkynyl group).

In CH_2Cl_2, excitation of the Au_{10} complexes **1**−**4** and **7** at the $S_0 \rightarrow S_1$ peak wavelength results in intense luminescence. The photophysical properties including the quantum yields (φ), observed lifetimes (τ_{obs}), and hence deduced radiative lifetime $\tau_r = 1/k_r = \varphi\tau_{obs}$ for the titled complexes are summarized in Table 1.

Table 1. Photophysical Properties of Au(I) Complexes 1−14 in CH_2Cl_2

	λ_{ab} /nm (10^{-4} ε/cm^{-1} M^{-1})	λ_{em} /nm	Φ^a	Φ^b	τ_{obs} /μs^c	τ_{rad}/ μs^d
1	370(2.8), 415(3.0)	599	0.18	0.10	0.26	0.88
2	370(2.81), 415(2.92)	605	1	0.68	2.25	2.25
3	365(2.58), 410(2.55)	572	0.66	0.09	0.91	1.38
4	364(1.90), 410(1.25)	589	0.22	0.16	0.98	4.45
7	363(3.03), 411(0.59)	582	0.26	0.32	0.45	1.73
9	411(2.92)	584	0.35	0.24	2.10	8.40
10	399(4.46)	570	0.20	0.64	0.86	4.30
11	387(4.51)	588	0.53	0.05	2.64	4.98
12	380(2.50)	579	0.25	0.01	0.96	3.84
13	380(3.67)	580	0.47	0.11	1.77	7.45
14	390(3.55)	570	0.41	0.89	0.92	2.24

[a]Measured in degassed CH_2Cl_2. [b]Measured in crystalline form at room temperature. [c]τ_{obs} denotes the observed lifetime obtained from degassed CH_2Cl_2. For complexes **1**−**4** and **7**, lifetime measurements are monitored at 600 nm. For complexes **9**−**14**, lifetime measurements are monitored at 510 nm. [d]τ_{rad} are deduced from lifetimes obtained from the degassed CH_2Cl_2. Coumarin 480 in methanol (λ_{excit} = 430 nm) and 4-(dicyanomethylene)-2-methyl-6-(paradimethylaminostyryl)-4*H*-pyran (DCM, λ_{max} = 615 nm, exciton) in methanol were used as standard dyes for quantum yield (Φ) measurements for complexes **1**−**4** and **7** and complexes **9**−**14**, respectively.

The magnitudes of the radiative decay rate constants are calculated to be around 10^5 s^{-1} for the decanuclear clusters, suggesting the luminescence is most likely associated with a spin-forbidden transition, i.e., phosphorescence. Moreover, the luminescence studies in aerated and degassed solution show rather small O_2 quenching of the emission intensity. For example, the phosphorescence quantum yield of **4** (in CH_2Cl_2) was measured to be 0.22 in the degassed solution, while it only decreased slightly to 0.20 upon aeration. Special attention may have to be paid to complex **2**, which shows the highest quantum yield up to unity in both aerated and degassed solution. The results manifest the uniqueness of the framework built by the Au_{10} supramolecules. Referring to Figure 10 for the excited state characteristics of complex **7** (vide infra), one can perceive that the emission chromophore originates from the central homometallic alkynyl clusters, which are largely shielded by the bulky ancillary and bridging ligands, thus avoiding O_2 quenching via a collision type of energy transfer. The similarity of the phosphorescence spectra of compounds **1**−**4** and **7** measured in solution and in the solid state (Figure 7) is in line with NMR spectral data discussed above and evidence that the cluster framework found in the crystalline phase remains intact in solution. The emission profile of complex **1** does not show any appreciable concentration dependence in the range of 10^{-5}−10^{-3} M (see Figure S10, Supporting Information). Taking into account the presence of two forms in solution of **1** according to the NMR spectroscopic measurements we tentatively propose that the minor tetranuclear isomer exhibits negligible emission in fluid medium.

Unlike Au_{10} complexes **1**−**4** and **7**, for which a single, nearly O_2 quenching free emission band was resolved, the Au_8 diphosphine derivatives **9**−**14** exhibit relatively complicated emission properties, in which certain complexes such as **11**−**13** appear to exhibit second emission tailing down to the red edge (see Figure 8). For example, Figure 9 shows the emission and excitation spectra of complex **11** in degassed and aerated CH_2Cl_2 solution.

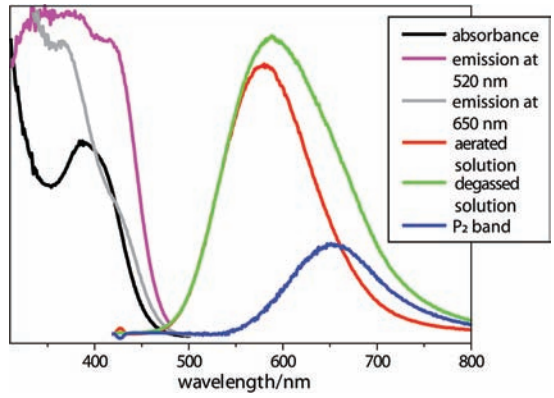

Figure 9. Normalized emission and excitation spectra of **11** (298 K, CH_2Cl_2). Emission spectrum in degassed solution (green) can be convoluted by the emission in aerated solution (the P_1 band, red) plus a fitted P_2 band maximized at 650 nm (blue, see text for detail).

We promptly recognized that the emission around the 650−800 nm region (defined as the P_2 band) was quenched significantly by O_2, while the major, short-wavelength emission in the spectral region of 470−650 nm (the P_1 band) remained nearly unchanged in intensity. Also, as shown in Figure 9, different excitation spectra were obtained when monitoring at each emission band. Further support is provided by the time-resolved measurement. In degassed solution, the emission of **11** at 510 nm reveals a single-exponential decay pattern with a lifetime of 2.64 μs. Upon monitoring at 700 nm, the time-resolved trace is best fitted by two single-exponential decay kinetics, in which minor (~15%) and major (~85%) decay components with lifetime of 2.60 and 4.15 μs, respectively, were resolved. Upon aeration, the 2.60 μs species decreases only slightly to 2.57 μs, while the 4.15 μs component was drastically reduced to 0.21 μs. The former was thus assigned to the residue of the P_1 band; evidently the latter should be attributed to the P_2 emission due to its dominant O_2 deactivation process. As depicted in Figure 9, we took the spectrum acquired in the aerated solution to be solely attributed to the P_1 emission band and then assumed the P_2 band to be a Gaussian function. We then performed a convolution procedure via optimizing both the peak wavelength and the bandwidth of the P_2 band. As a result, a P_2 emission band maximized at 650 nm was resolved.

dx.doi.org/10.1021/ic300856h | Inorg. Chem. 2012, 51, 7392−7403

Similar results were obtained for **12** and **13**, although the difference in spectra and relaxation dynamics between degassed and aerated CH_2Cl_2 is not as significant as that of **11** (see Table 2

Table 2. Lifetime Measurements of Complexes 11−13 Monitored at 510 and 710 nm in Degassed and Aerated CH_2Cl_2 Solutions at 298 K

	τ_{obs} /μs[a] (degassed)	τ_{obs} /μs[b] (degassed)	τ_{obs} /μs[a] (aerated)	τ_{obs} /μs[b] (aerated)
11	2.64 (1.0)	4.15 (0.83)[c]	2.58 (1.0)	0.21 (0.83)[c]
		2.60 (0.17)		2.57 (0.17)
12	0.96 (1.0)	3.18 (0.68)	0.96 (1.0)	0.19 (0.66)
		1.01 (0.32)		0.98 (0.34)
13	1.77 (1.0)	3.50 (0.78)	1.75 (1.0)	0.20 (0.74)
		1.81 (0.22)		1.78 (0.26)

[a]Monitored at 510 nm. [b]Monitored at 700 nm. [c]Number in the parentheses indicates the pre-exponential term (t = 0).

for decay dynamics and Figures S11 and S12 in the Supporting Information for the emission spectra). The results are consistent with the earlier proposal of interconversion between two structural types according to the ^{1}H NMR measurement for complexes **11−13**. It seems like that the alkynyl ligands in complexes **11−13** are less bulky than in the rigid **8−10** and **14** complexes and hence render higher opportunity to undergo isomerization in solution. As shown in Scheme 4, the latter isomer is a relatively open structure, which may allow unhampered access for O_2 toward the emissive chromophore, facilitating the O_2 quenching process. Moreover, since both phosphorescence bands reveal instant rise dynamics, i.e., <300 ps of the instrument response time, these two emission bands lack any precursor−successor type of relationship. Therefore, interconversion between these two species in the excited state is not possible. In the solid crystalline the population of this open octanuclear isomer in **11−13** seems negligible, as evidenced by the disappearance of the P_2 band at >650 nm (see Figure 8B).

Computational Results. We investigated the structural and photophysical characteristics of the Au^I_{10} clusters **1−7** and Au^I_8 clusters **8−14** by means of density functional calculations. The geometries of all clusters were first optimized at the PBE0-DFT level of theory. The structural motifs of both types of clusters (**1−7** and **8−14**) were reproduced well by DFT. In the case of complex **1**, where the experimentally determined intermetallic distances were found to vary between 2.8804(5) and 3.0937(5) Å, the corresponding minimum and maximum Au−Au distances in the DFT-optimized structure are 2.99 and 3.13 Å. The slight elongation of the shortest distances in comparison to the X-ray structure is expected since the effects of the solid-state packing are missing in the calculations. For the cationic complexes **13** and **14**, the theoretical Au−Au distances of 2.92−3.25 (**13**) and 2.92−3.24 Å (**14**) are also in good agreement with the experimentally observed intermetallic distances of 2.8937(9)−3.2834(8) (**13**) and 2.8743(3)−3.2916(4) Å (**14**). Concerning the structural interconversion proposed above for clusters **10−13**, the energy difference between two structural forms shown in Scheme 4 is only 20−49 kJ/mol depending on the complex. The low-energy difference between the two types of self-assembling clusters points to the possibility of the coexistence of the two structural forms at room temperature.

The photophysical features of the complexes were investigated by means of time-dependent DFT calculations (PBE0-TDDFT). First, the singlet excitation spectrum of each complex at the optimized ground state geometry was calculated. Next, the geometry of the lowest energy triplet state of each complex was optimized to investigate their emission features. The photophysical data obtained at the PBE0-TDDFT level of theory are listed in Table 3, and the excited state transition densities of the

Table 3. Computational Photophysical Results for Clusters 1−14 (PBE0 TD-DFT level of theory)

	λ_{ab} $S_0 \rightarrow S_1$ (nm)		λ_{ab} $S_0 \rightarrow S_2$ (nm)		λ_{em} $T_1 \rightarrow S_0$ (nm)	
	theor[a]	exp	theor	exp	theor	exp
1	418 (0.22)	415	378 (0.15)	370	557	599
2	406 (0.41)	415	370 (0.06)	370	581	605
3	396 (0.28)	410	357 (0.14)	365	525	572
4	399 (0.35)	410	330 (0.13)	370	549	589
5	403 (0.34)		327 (0.13)		581	
6	390 (0.41)		352 (0.15)		569	
7	410 (0.30)	411	338 (0.13)	363	528	582
8	402 (0.46)				496	
9	390 (0.41)	411			480	584
10	387 (0.41)	399			474	570
11	390 (0.45)	387			486	588
12	386 (0.46)	380			487	579
13	403 (0.47)	380			501	580
14	405 (0.53)	390			498	570

[a]Wavelengths in nanometers, oscillator strengths given in parentheses.

representative complexes **7** and **14** (R = $C_{10}H_{17}O$) are shown in Figure 10. The transition densities of the other clusters **1−6** and

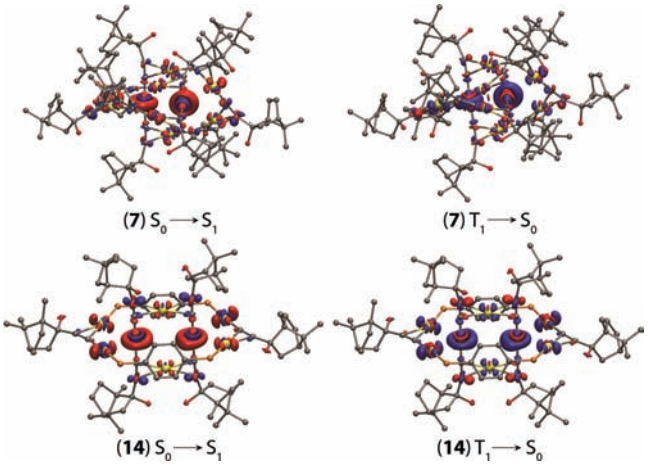

Figure 10. Transition densities for the lowest energy singlet excitation ($S_0 \rightarrow S_1$) and lowest energy triplet emission ($T_1 \rightarrow S_0$) of complexes **7** and **14** (R = $C_{10}H_{17}O$; isovalue 0.002 au). During the transition, the electron density increases in the blue areas and decreases in the red areas.

8−13 are very similar to those in clusters **7** and **14**, respectively (the densities are plotted in Figures S13 and S14 in the Supporting Information). The calculated $S_0 \rightarrow S_1$ and $S_0 \rightarrow S_2$ excitation energies are generally in good agreement with the experimental absorption data. For both Au^I_{10} cluster **7** and Au^I_8 cluster **14**, the lowest energy $S_0 \rightarrow S_1$ excitation is a metal-centered Au→Au transition mixed with a transfer of electron density to the alkynyl π^* orbitals. In the case of the Au^I_{10} cluster **7**, the $S_0 \rightarrow S_2$ excitation energy is generally rather similar to the lowest energy excitation but with increased MLCT contribution, in accordance with the higher excitation energy (transition

dx.doi.org/10.1021/ic300856h | Inorg. Chem. 2012, 51, 7392−7403

densities for the $S_0 \rightarrow S_2$ excitation of the cluster **7** are illustrated in Figure S15, Supporting Information). The $T_1 \rightarrow S_0$ emission characteristics of clusters **7** and **14** are practically opposite to the corresponding $S_0 \rightarrow S_1$ excitations in terms of transition densities. However, there are notable differences in the accuracy of the predicted emission wavelengths. The studied clusters show rather large Stokes shifts of about 160−200 nm, but this could be reproduced only for clusters Au^I_{10} **1**−**7**. In this case, geometry relaxation of the T_1 state leads to clear structural changes, although the general structural motif is retained. For example, in the case of cluster **7**, the Au−Au distances decrease from 2.97−3.17 to 2.88−3.05 Å, the Au atoms are slightly rearranged with respect to each other, and the configuration of the alkynyl ligands is clearly affected as well. In contrast, in the Au^I_8-type cluster **14**, the Au−Au distances do change from 2.92−3.24 to 2.91−3.33 Å but the configuration of the alkynyl ligands is hardly affected. The triplet emission wavelengths predicted for clusters **8**−**14** vary from 474 to 501 nm, while the experimentally observed wavelengths are 570−588 nm. For comparison, in the case of the closely related $Au^I_6Cu^I_2$ clusters,[8] the observed Stokes shifts for the triplet emission were less than 100 nm and the PBE0-TDDFT predicted values were in good agreement with the experimental ones. Similar to clusters **8**−**14** studied here, relaxation of the triplet state geometries mainly resulted in a minor movement of the metal atoms for all Au^I_6−Cu^I_2 clusters. Hence, the relatively large difference in the calculated and observed triplet emission wavelengths for clusters **8**−**14** most likely results from the fact that despite several different approaches we were unable to discover a relaxed T_1 geometry that would have reproduced the experimentally observed large Stokes shift.

CONCLUSION

In summary, a family of unprecedented homoleptic gold(I) alkynyl clusters was effectively prepared using a very simple synthetic route. The discrete molecular compounds $(AuC_2R)_{10}$ (R = 9-fluorenol (**1**), diphenylmethanol (**2**), 2,6-dimethyl-4-heptanol (**3**), 3-methyl-2-butanol (**4**), 4-methyl-2-pentanol (**4**), 1-cyclohexanol (**6**), 2-borneol (**7**)), which contain a unique catenane metal core with two interlocked 5-membered rings, became accessible only when the hydroxyaliphatic alkynyl ligands were employed. This underlines how the subtle stereochemical and electronic properties of the ligand environment strongly affect the assembly processes of the polymetallic entities. Treatment of the decanuclear clusters **1**−**7** with gold−diphosphine complex $[Au_2(PPh_2{-}C_6H_4{-}PPh_2)_2]^{2+}$ led to octanuclear cationic derivatives $[Au_8(C_2R)_6(PPh_2{-}C_6H_4{-}PPh_2)_2]^{2+}$ (**8**−**14**), which consist of the planar tetranuclear $\{Au_4(C_2R)_4\}$ units coupled with two $[AuPPh_2{-}C_6H_4{-}PPh_2(AuC_2R)]^+$ fragments.

NMR and ESI-MS spectroscopic studies showed that the Au_{10} clusters **1**−**7** retain their structures in solution, though **1** demonstrates certain concentration-dependent isomerization. The octanuclear diphosphine successors **8**−**14** showed different behavior in fluid medium. Compounds **8**, **9**, and **14** are structurally rigid in solution, while their congeners **10**−**13** exhibit complicated dynamic behavior.

Both types of clusters, **1**−**7** and **8**−**14**, are intense triplet luminophores in solution and in the solid state with the maximum quantum yield approaching 100% (**2** in solution). Phosphorescence of the titled compounds, observed in the range 570−605 nm, is poorly affected by O_2 quenching due to the sterical protection of the emissive centers by the organic ligands. Photophysical investigations were supported by DFT computational studies, which provided information on the electronic transitions responsible for luminescence. For both Au^I_{10} and Au^I_8 clusters, metal-centered Au → Au charge transfer transitions mixed with some π-alkynyl MLCT character play a dominant role in their photoemission properties.

ASSOCIATED CONTENT

Supporting Information

X-ray crystallographic data in CIF format for **1**, **13**, and **14**; ESI-MS spectra of **1**−**14**, additional NMR spectroscopic data; additional computational results; optimized Cartesian coordinates of the studied systems in atomic units. This material is available free of charge via the Internet at http://pubs.acs.org.

AUTHOR INFORMATION

Corresponding Author

*E-mail: igor.koshevoy@uef.fi (I.O.K.), chop@ntu.edu.tw (P.-T.C.).

Notes

The authors declare no competing financial interest.

ACKNOWLEDGMENTS

We thank the University of Eastern Finland (Finnish-Russian collaborative project and Spearhead project), Academy of Finland (grant 138560/2010, A.J.K.), Russian Foundation for Basic Research (grants 11-03-00541-a and 11-03-92010-NNS-a), and St. Petersburg State University (grant 12.37.132.2011).

REFERENCES

(1) (a) Yam, V. W.-W.; Lo, K. K.-W.; Wong, K. M.-C. *J. Organomet. Chem.* **1999**, *578*, 3−30. (b) Yam, V. W.-W.; Wong, K. M.-C. *Top. Curr. Chem.* **2005**, *257*, 1−32. (c) Yam, V. W.-W.; Cheng, E. C.-C. *Top. Curr. Chem.* **2007**, *281*, 269−309. (d) López-de-Luzuriaga, J. M. Luminescence of Supramolecular Gold-Containing Materials. In *Modern Supramolecular Gold Chemistry*; Laguna, A., Ed.; Wiley-VCH: Weinheim, 2008; pp 347−402. (e) Lu, W.; Kwok, W.-M.; Ma, C.; Chan, C. T.-L.; Zhu, M.-X.; Che, C.-M. *J. Am. Chem. Soc.* **2011**, *133*, 14120−14135.

(2) He, X.; Yam, V. W.-W. *Coord. Chem. Rev.* **2011**, *255*, 2111−2123.

(3) Au, V. K.-M.; Wong, K. M.-C.; Tsang, D. P.-K.; Chan, M.-Y.; Zhu, N.; Yam, V. W.-W. *J. Am. Chem. Soc.* **2010**, *132*, 14273−14278.

(4) (a) Schmidbaur, H. *Gold Bull.* **2000**, *33*, 3−10. (b) Schmidbaur, H.; Schier, A. *Chem. Soc. Rev.* **2008**, *37*, 1931−1951.

(5) (a) Mingos, D. M. P.; Yau, J.; Menzer, S.; Williams, D. J. *Angew. Chem., Int. Ed.* **1995**, *34*, 1894−1895. (b) Yip, S.-K.; Cheng, E. C.-C.; Yuan, L.-H.; Zhu, N.; Yam, V. W.-W. *Angew. Chem., Int. Ed.* **2004**, *43*, 4954−4957. (c) Chui, S. S. Y.; Ng, M. F. Y.; Che, C.-M. *Chem.—Eur. J.* **2005**, *11*, 1739−1749. (d) Constable, E. C.; Housecroft, C. E.; Neuburger, M.; Schaffner, S.; Shardlow, E. J. *Dalton Trans.* **2007**, 2631−2633. (e) Hooper, T. N.; Green, M.; Russell, C. A. *Chem. Commun.* **2010**, *46*, 2313−2315. (f) Koshevoy, I. O.; Lin, C.-L.; Karttunen, A. J.; Haukka, M.; Shih, C.-W.; Chou, P.-T.; Tunik, S. P.; Pakkanen, T. A. *Chem. Commun.* **2011**, *47*, 5533−5535. (g) Himmelspach, A.; Finze, M.; Raub, S. *Angew. Chem., Int. Ed.* **2011**, *50*, 2628−2631. (h) Puddephatt, R. J. *Chem. Soc. Rev.* **2008**, *37*, 2012−2027. (i) Schmidbaur, H.; Schier, A. *Chem. Soc. Rev.* **2012**, *41*, 370−412.

(6) (a) Coates, G. E.; Parkin, C. *J. Chem. Soc.* **1962**, 3220−3226. (b) Vicente, J.; Gil-Rubio, J.; Barquero, N.; Jones, P. G.; Bautista, D. *Organometallics* **2008**, *27*, 646−659. (c) Buschbeck, R.; Low, P. J.; Lang, H. *Coord. Chem. Rev.* **2011**, *255*, 241−272.

(7) (a) Vicente, J.; Chicote, M.-T.; Alvarez-Falcon, M. M.; Jones, P. G. *Organometallics* **2005**, *24*, 4666−4675. (b) Hogarth, G.; Alvarez-Falcon, M. M. *Inorg. Chim. Acta* **2005**, *358*, 1386−1392. (c) Ferrer, M.; Mounir, M.; Rodriguez, L.; Rossell, O.; Coco, S.; Gomez-Sal, P.; Martin, A. *J.*

Organomet. Chem. **2005**, *690*, 2200−2208. (d) Siemeling, U.; Rother, D.; Bruhn, C. *Chem. Commun.* **2007**, 4227−4229. (e) He, X.; Cheng, E. C.-C.; Zhu, N.; Yam, V. W.-W. *Chem. Commun.* **2009**, 4016−4018. (f) Kilpin, K. J.; Horvath, R.; Jameson, G. B.; Telfer, S. G.; Gordon, K. C.; Crowley, J. D. *Organometallics* **2010**, *29*, 6186−6195.
(8) Koshevoy, I. O.; Lin, C.-L.; Karttunen, A. J.; Jänis, J.; Haukka, M.; Tunik, S. P.; Chou, P.-T.; Pakkanen, T. A. *Chem.—Eur. J.* **2011**, *17*, 11456−11466.
(9) Uson, R.; Laguna, A.; Laguna, M. *Inorg. Synth.* **1989**, *26*, 85−91.
(10) Baldwin, R. A.; Cheng, M. T. *J. Org. Chem.* **1967**, *32*, 1572−1577.
(11) Kaldis, J. H.; Morawietz, P.; McGlinchey, M. J. *Organometallics* **2003**, *22*, 1293−1301.
(12) (a) Koshevoy, I. O.; Koskinen, L.; Haukka, M.; Tunik, S. P.; Serdobintsev, P. Y.; Melnikov, A. S.; Pakkanen, T. A. *Angew. Chem., Int. Ed.* **2008**, *47*, 3942−3945. (b) Koshevoy, I. O.; Lin, Y.-C.; Karttunen, A. J.; Haukka, M.; Chou, P.-T.; Tunik, S. P.; Pakkanen, T. A. *Chem. Commun.* **2009**, 2860−2862.
(13) *APEX2-Software Suite for Crystallographic Programs*; Bruker AXS, Inc.: Madison, WI, 2009.
(14) Sheldrick, G. M. *Acta Crystallogr., Sect. A* **2008**, *A64*, 112−122.
(15) Palatinus, L.; Chapuis, G. *J. Appl. Crystallogr.* **2007**, *40*, 786−790.
(16) Farrugia, L. J. *J. Appl. Crystallogr.* **1999**, *32*, 837−838.
(17) Sheldrick, G. M. *SADABS-2008/1-Bruker AXS area detector scaling and absorption correction*; Bruker AXS: Madison, WI, 2008.
(18) Spek, A. L. *PLATON, A Multipurpose Crystallographic Tool*; Utrecht University: Utrecht, The Netherlands, 2005.
(19) Nardelli, M. *J. Appl. Crystallogr.* **1999**, *32*, 563−571.
(20) (a) Perdew, J. P.; Burke, K.; Ernzerhof, M. *Phys. Rev. Lett.* **1996**, *77*, 3865−3868. (b) Adamo, C.; Barone, V. *J. Chem. Phys.* **1999**, *110*, 6158−6170.
(21) Weigend, F.; Ahlrichs, R. *Phys. Chem. Chem. Phys.* **2005**, *7*, 3297−3305.
(22) Andrae, D.; Häußermann, U.; Dolg, M.; Stoll, H.; Preuss, H. *Theor. Chem. Acc.* **1990**, *77*, 123−141.
(23) Schäfer, A.; Horn, H.; Ahlrichs, R. *J. Chem. Phys.* **1992**, *97*, 2571−2577.
(24) (a) Eichkorn, K.; Treutler, O.; Öhm, H.; Häser, M.; Ahlrichs, R. *Chem. Phys. Lett.* **1995**, *240*, 283−290. (b) Sierka, M.; Hogekamp, A.; Ahlrichs, R. *J. Chem. Phys.* **2003**, *118*, 9136−9148. (c) Eichkorn, K.; Weigend, F.; Treutler, O.; Ahlrichs, R. *Theor. Chem. Acc.* **1997**, *97*, 119−124. (d) Weigend, F. *Phys. Chem. Chem. Phys.* **2006**, *8*, 1057−1065.
(25) (a) Furche, F.; Rappoport, D. Density Functional Methods for Excited States: Equilibrium Structure and Electronic Spectra. In *Computational Photochemistry*; Olivucci, M., Ed.; Elsevier: Amsterdam, 2005; pp 93−128. (b) Furche, F.; Ahlrichs, R. *J. Chem. Phys.* **2002**, *117*, 7433−7447. (c) van Wüllen, C. *J. Comput. Chem.* **2011**, *32*, 1195−1201.
(26) Ahlrichs, R.; Bär, M.; Häser, M.; Horn, H.; Kölmel, C. *Chem. Phys. Lett.* **1989**, *162*, 165−169.
(27) Vicente, J.; Chicote, M.-T.; Alvarez-Falcon, M. M.; Jones, P. G. *Organometallics* **2005**, *24*, 5956−5963.
(28) Montano, P. A.; Zhao, J.; Ramanathan, M.; Shenoy, G. K.; Schulze, W. *Physica B* **1989**, *158*, 242−244.